In situ label-free static cytometry by monitoring spatiotemporal fluctuations of image gray values

Ishay Wohl
Naomi Zurgil
Yaron Hakuk
Maria Sobolev
Moti Galmidi
Mordechai Deutsch

In situ label-free static cytometry by monitoring spatiotemporal fluctuations of image gray values

Ishay Wohl, Naomi Zurgil, Yaron Hakuk, Maria Sobolev, Moti Galmidi, and Mordechai Deutsch*
Bar Ilan University, The Biophysical Interdisciplinary Schottenstein Center for the Research and Technology of the Cellome, Physics Department, Ramat-Gan 5290002, Israel

Abstract. Spatiotemporal fluctuation of homogeneity and randomness of gray values within an image was explored and utilized as a label-free means for cell examination. This was done by utilizing a user-friendly combination of simple bright field microscope and Cytocapture dish, wherein cells are individually held, each within a picoliter optical chamber, forming an array of cells to be repeatedly measured over time and biomanipulated *in situ* at single-cell resolution. First, the measured gray level information entropy (GLIE) was used and, based on the fact that living cells are not in a state of thermodynamic equilibrium but rather in a metastable state, two fluctuation-sensitive measures were proposed and examined: ASDE—the spatial average of temporal standard deviation (SD) of GLIE, and AA—the average time autocorrelation of GLIE. System performance was validated on cell-free solutions. This was followed by examining the performance of the measures AGLIE, ASDE, and AA to distinguish among individual live-still, dead and live cells from various cell lines, as well as between cells which were and were not induced to differentiate. Results, which were obtained on four types of cells, indicate advantages of the proposed measures which are believed to be significant additions to the microscope-based probe-free toolbox. © *2015 Society of Photo-Optical Instrumentation Engineers (SPIE)* [DOI: 10.1117/1.JBO.20.10.105013]

Keywords: biological optics; image analysis; digital imaging; microscopy; scattering; Fourier transforms.

Paper 150431R received Jun. 24, 2015; accepted for publication Aug. 25, 2015; published online Oct. 27, 2015.

1 Introduction

The tremendous contribution of microscopy, in general, and of fluorescence microscopy in particular, to fundamental research in life sciences is obvious and needs no clarification. However, molecular specificity, one of its major advantages, cannot be addressed with current label-free methods, therefore, in most cases, it calls for the use of exogenous fluorophores, introduced into the investigated cells in order to enhance the "visibility" of a component or feature of interest within the cell or its membrane. There are two pivotal limitations to labeling cells with exogenous fluorophores[1]: (a) exogenous fluorophores may interfere with the physiology of the hosting cell, and hence bias the results and (b) the fluorescent label, especially when related to a living cell, tends to bleach while illuminated. Therefore, though at present its ability to trace subcellular events is much more modest, the label-free microscopy (LFM) approach is significantly developed in an effort to address these shortcomings, enabling measurement in standard culture conditions without requiring any further manipulation.[2,3] Recruitment of LFM and other nonmicroscopy label-free measurements for research and drug discovery has become more and more common in the last decade.[2,4]

Of these LFM approaches, pixel-based analysis of bright field computerized images affords definition of characteristic features of gray value distribution within an image.[5–7] In this context, we note the fundamental work of Haralick et al.,[8] in which the term entropy is borrowed from physics to define an index of textural entropy (TE) for the gray values within an image: $\text{Textural Entropy} = -\sum_i \sum_j p(i,j) \log[p(i,j)]$, where $p(i,j)$ stands for the incidence of two gray values (i and j) at a specific predetermined angle and distance where TE, which reflects the lack of homogeneity and randomness in the analyzed image, is one of 14 gray-level co-occurrence matrix (GLCM) Haralick indices.

Several studies have investigated the relationship between clinical situations and GLCM, for instance, cellular senescence,[9] apoptosis,[10] and activation of lymphocytes[11,12] and GLCM values obtained from measurement within the nuclear image of postfixation stained cells. Cellular senescence and apoptosis resulted in a decrease in homogeneity of image gray value appearance and an increase in nuclear textural entropy values,[9,10] while on the other hand, activation of lymphocytes yielded an increase in homogeneity and a decrease in textural entropy of cell nuclei.[11,12]

Another approach to describe the level of homogeneity and complexity of gray values constructing an image was proposed by Gonzalez and Woods.[13] They relied on information entropy formulation and described the average information E in the measured pixels in bit units: $E = -\sum p_i \log_2 p_i$, where p_i stands for the occurrence of pixels with a specific gray value i within the inspected image field. This was further realized in flow cytometry by Wiedemann et al.[14] who calculated Gonzalez's E values on 25 pixels of a cell image acquired during flow. This was compared to the results of viability tests performed on the same cells during flow as well. Though sensitivity and specificity of E values are not presented in their work, they indeed show that E values of dead cells are higher than those of living cells, hence enabling presentation of two distinct cell populations. Their experimental setup of flow cytometry, however, was not suitable for exploring spatiotemporal fluctuations of their calculated index.

---

*Address all correspondence to: Mordechai Deutsch, E-mail: motti.jsc@gmail.com

These studies explored the possible relation between physiological states of cells and static textural entropy of gray values within the cell image, overlooking the dynamic and fluctuating aspects of a cell, which in turn regulates the fluctuating nature of the homogeneity and randomness of gray values within the cell image.

Complementary to the above static measures, this study examines the informative value of their fluctuations. In particular, based on the hypothesis that living cells are not in a state of thermodynamic equilibrium, but rather in a metastable state,[15–17] the proposed approach relies on the fluctuating nature of the static measure gray level information entropy (GLIE) and offers two novel dynamic measures: (a) ASDE—the spatial average of the temporal standard deviation (SD) of GLIE and (b) AA—the average time autocorrelation of GLIE. Performance of these two was exemplified in contrast to that of GLIE on various states (dead and live nondifferentiated and differentiated) of U-937 cells at single cell resolution. In addition, the power spectrum of GLIE was analyzed using discrete Fourier transform (DFT). Results were then further confirmed in two T cell lines (Jurkat and Molt-4), and on embryonic HEK293 cells as well, and indicated that precision in differentiating between cells in various states was greatest when based on the proposed fluctuation-based measures.

2 Materials and Methods

2.1 Materials

Complete medium (medium): RPMI-1640, Dulbecco's Modified Eagle Medium (DMEM), heat-inactivated fetal calf serum (FCS), penicillin, streptomycin, glutamine, sodium pyruvate, 4-(2-hydroxyethyl)-1-piperazineethanesulfonic acid (HEPES), and trypsin-EDTA solution B were obtained from biological industries (Kibbutz Beit Haemek, Israel). Propidium iodide (PI) and phorbol myristate acetate (PMA) were obtained from Sigma-Aldrich (St. Louis, Missouri).

2.1.1 Cell lines

Human promonocytic U-937 cells (ECACC, United Kingdom) as well as Molt-4 and Jurkat T-lymphoblast cell lines were maintained in RPMI-1640 medium supplemented with 10% FCS, 100 U/ml penicillin, 100 μg/ml streptomycin, 2% glutamine, 2% sodium pyruvate, and 2% HEPES. Cells were maintained

in completely humidified air with 5% CO_2 at 37°C. Before use, exponentially growing cells were obtained, washed, and suspended in phosphate-buffered saline (PBS) at a concentration of $1.5–2.0 \times 10^6$ cells/ml.

HEK293 cell line was grown as a monolayer in a high glucose DMEM medium supplemented with 10% FCS, 100 U/mL penicillin, 100 μg/mL streptomycin, 2% glutamine, and 2% sodium pyruvate. Cells were grown in a completely humidified atmosphere containing 5% CO_2 at 37°C. For preparation of HEK293 cell suspension, cells were harvested by incubation for 3 min at room temperature with 0.25% trypsin-EDTA solution B, followed by washing and suspending in PBS at a concentration of $1.5–2.0 \times 10^6$ cells/ml.

2.1.2 Petri dish-based Cytocapture and related operations

A commercial Cytocapture imaging dish (joint venture of Zell-Kontakt GmbH, Nörten-Hardenberg, Germany and Molecular-Cytomics Inc., Boston) was used (Fig. 1). For cell loading, 40 μL of cell suspension (2.5×10^6 cells/mL) in PBS or HEPES buffer were loaded on top of the picoliter well (PW) array (Fig. 1, middle panel) and cells were allowed to settle by gravity for 5–10 min. Then 500 μL of buffer was added gently to the medium exchange region around the array. The imaging dish was mounted on the microscope stage and measured. An example of cells within their PWs is shown in the right panel of Fig. 1.

For each measurement of cell free solution and cells, two Cytocapture dishes were used—in each of which 10 PWs were sampled.

2.1.3 Induction of cell death

Cell death was induced by serum deprivation. Cells were incubated for 48 h in incomplete RPMI-1640 (without FCS), then washed, suspended in HEPES buffer (0.1 M HEPES, pH 7.4; 1.4 M NaCl; 25 mM $CaCl_2$) and maintained for 12 h, then washed again and loaded on the array.

Cell viability and plasma membrane integrity were evaluated by staining with PI. PI (final concentration 2.5 μg/ml) was added to the cells within the PW array and incubated for 10 min in the dark at room temperature. The excitation filter was 470 to 490 nm, dichroic mirror 505-nm long pass, and emission filter 510 to 530 nm.
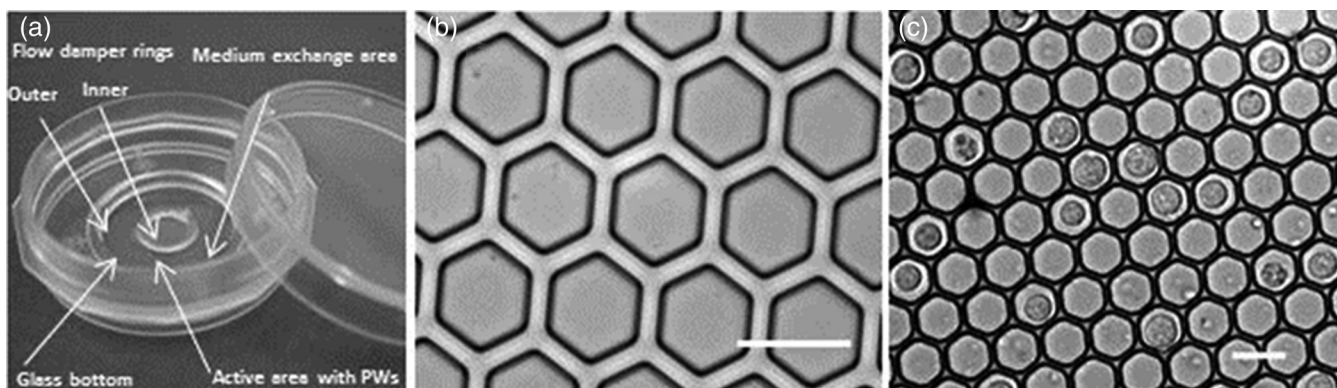
Fig. 1 The Cytocapture dish. (a) Tiled view of the dish. (b) Picoliter wells (PWs) on the glass bottom of a Cytocapture dish. PWs are filled with complete RPMI-1640 medium. Upper edges of PWs are set within the microscope focal plane. (c) Molt-4 cells within the 20 μm diameter/10 μm deep honeycomb array. Bars indicate 20 μm.

2.1.4 *Phorbol myristic acetate-induced U-937 differentiation*

U-937 promonocyte cells were incubated in completely humidified air with 5% CO_2 at 37°C for 24 h, in tissue culture flasks containing complete medium in the presence of 1 ng/ml PMA to induce differentiation into monocyte-macrophage-like cells.

2.2 *Measurement System*

2.2.1 *Microscope*

Images were acquired using a motorized Olympus inverted IX81 microscope (Tokyo, Japan). The microscope is equipped with a submicron Marzhauser Wetzlar motorized stage-type SCAN-IM, with an Lstep controller (Wetzlar-Steindorf, Germany) and a filter wheel, including the fluorescence cube (excitation filters, dichroic mirrors, and emission filters, respectively), all filters were obtained from Chroma Technology Corporation (Brattleboro, Vermont). A 100× oil objective NA = 1.35 and 60× objective NA = 0.70 were used without oil immersion, since its density tends to fluctuate and consequently the intensity of light propagates through it as well.[18] Nevertheless, the quality of the study was not mitigated with this approach, as tracking pixel-based fluctuation was the purpose, rather than image-analysis-based investigation, and though the resolution of the image would be lower than with oil, it would be of no consequence since the data are binned later during image processing. A microscope halogen 12 V/100 W lamp was used as a light source with a control box which diminishes intense electrical noise and heat from the microscope frame.

2.2.2 *Image/data acquisition*

A 12-bit cooled, highly sensitive ORCA II C4742-98 camera (Hamamatsu, Japan) was used for image and data acquisition. Image acquisition time was 1 ms, in a 16-bit TIF format, each having 1344×1024 pixels, and a physical dimension of 87.27×66.49 μm^2 at 100× magnification and 147.69×112.53 μm^2 at 60× magnification on the microscope working plane. Illumination of the sample was synchronized with acquisition time using a controllable electronic shutter.

2.2.3 *Image processing*

Acquired stacks of 200 16-bit TIF images were used for calculation of GLIE, using MATLAB® R2013a software (MathWorks Inc. Natick, Massachusetts). Using MATLAB, 12-bit images with 4096 possible gray values were converted into 682 possible gray value images by reducing every six successive gray values to one new gray value.

The GLIE calculation equation used was:

$$\text{GLIE} = -\sum_{i=1}^{i=N} P_i \ln P_i, \tag{1}$$

where P_i stands for the occurrence of specific gray level value i. $\sum P_i = 1$ and N are the number of different gray values, both within the inspected field. For the sake of clarity, from here on, the expression entropy will stand for GLIE.

Practically speaking, in this study, the spatiotemporal aspect of GLIE is of interest. To that end, a region of interest (ROI) consisting of 100×100 pixels at the center of the acquired PW image was defined for processing. Each field of view was acquired 200 times at 0.5 s intervals, and was indexed by its serial time point (1 to 200), all together yielding the temporal aspect of GLIE within a ROI. Next, the spatial aspect of GLIE within the ROI was examined by dividing the 100×100 pixels of a ROI into 400 subgroups, each consisting of 5×5 pixels from which the 25 pixel-based spatial GLIE (GLIE25) was calculated for each of the 200 time points. Hence, for each time point, a GLIE25 map was compiled from 400 GLIE25 values, reflecting the spatial distribution aspect of GLIE within a ROI. Practically, a discrete bins, rather than a sliding windows approach was realized though the latter might yield a higher resolution map of GLIE.

ROIs were chosen (a) at the center of a PW for investigation of cell-free solutions and (b) at the image center of a cell occupying a PW, for investigation of cells within the PWs. From this spatiotemporal data, the following measures were calculated:

Time-space averaged GLIE: A two-step averaging (time and space) of GLIE25. First, each GLIE25 was averaged over the 200 time points yielding 400 aGLIE values of time-based averaged GLIE25. Then the average of these 400 values was calculated as well, all together yielding the AGLIE value of a ROI. Since GLIE might be fluctuative in nature (yes/no randomly), the proposed measure AGLIE is perceived as an accurate evaluation like the GLIE measure used by others.[14] Hence, all consequent results and conclusions will be used to identify the nature of the GLIE measure.

Space averaged temporal standard deviation of entropy: This is a newly proposed measure determined by calculating the temporal SD of 200 time serial GLIE25 values (SD25), yielding 400 values of SD25. Then the average of these 400 SD25 values is defined as the ASDE value of a ROI.

Space averaged autocorrelation: This is a newly proposed measure consisting of two-step calculations. First, calculation of A25, the time autocorrelation of 200 GLIE25 values utilizing the one-lag time unit autocorrelation (r) equation (MathWorks Inc. Natick, Massachusetts):

$$r = \frac{N}{N-1}\sum_{t=1}^{N-1}(x_t - \bar{x})(x_{t+1} - \bar{x}) / \sum_{t=1}^{N}(x_t - \overline{x})^2, \tag{2}$$

where N is the total number of GLIE25 measurements, i.e., 200, performed on the same subgroup of 5×5 pixels, t is the serial number of a single GLIE25 measurement (one out of 200), x_t is the GLIE25 value of the t measurement, x_{t+1} is the succeeding GLIE25 value, i.e., of the $t + 1$ measurement, and $\bar{x}$ is the average GLIE25 value taken over the 200 measurements. Second, averaging these A25 time correlation values over the 400 unit cells within a ROI.

The power spectrum of GLIE was calculated by applying DFT on the time dependence GLIE discrete values, (using MATLAB R2013a software, MathWorks Inc. Natick, Massachusetts), from which a new measure, AP, was calculated as follows:

Average power spectrum amplitude: This is the average power amplitude of the frequency range <0.5 Hz.

2.2.4 *Data analysis and statistics*

The acquired data within ROIs were exported to Excel spreadsheets (Microsoft Inc., Redmond, Washington) for graph and table presentation and statistical analysis. Significance of differences between groups was calculated using analysis of

variance single factor function, with statistical significance set at $p < 0.05$.

3 Results and Discussion

3.1 *System Performance Validation*

Feasibility of the proposed approach, that is application of fluctuation-based measures as a probe-free indicator in light microscopy, was comprehensively examined. Specifically, the dependency of AGLIE, ASDE, and AA measures upon deviations one might encounter in routine use of light microscopy was examined in order to define the consequent limitations and thresholds of said measures. Relevant experiments were performed as described in Materials and Methods, on a Cytocapture dish filled with cell-free media and placed with its microcavity edge plane adjusted to the microscope working plane, yielding a focused image.

The influencing factors considered were electrical noise, light intensity, incorrect vertical sample placement, and type of sample hosting liquid.

ASDE and AA were found to be more indifferent than GLIE to light intensity, vertical sample placement (at the range $+2 \rightarrow -2\ \mu$m around the working plane), and sample hosting liquid. Results of these feasibility tests seem to suggest that ASDE and AA measures are more appropriate than AGLIE for evaluating true changes occurring in cells, since they allow attribution of measured changes to intracellular physiological alteration or fluctuation, rather than to inherent fluctuation in the measuring system. For detailed description of experiments performed, results obtained and their analysis, see Appendix.

3.2 *Measurements of Averaged Gray Level Information Entropy, Averaged Temporal Standard Deviation of Entropy, and Averaged Autocorrelation in Live and Dead U-937 Cells*

This experiment aimed to evaluate the ability of AGLIE, ASDE, and AA to distinguish between dead and live cells. The rationale behind this is that cell physiology, which is a major factor in determining the time-dependent physiochemical states of cell content, is expected to be spatiotemporally reflected within the cell content and its consequent optical features, which in turn, can be effectively traced by either said fluctuative measure, ASDE, or AA.

Two extreme physiological states were preferred: live and dead cells, which are also distinguishable by the well-established PI staining method used as a complementary reference examination. Figure 2 presents a transmitted light image of a field of PWs containing cells ($\times$100, bright field) beside the corresponding PI fluorescence image of the same field.

Three populations of U-937 cells were examined:

1. Dead-cell population (induced by serum deprivation).

2. Mostly ($\sim$97%) live-cell population.

3. Mixture of the two above populations.

In all cases, frequency of dead cells within a mixture was assured by counting PI-stained cells. For each of the three populations, AGLIE, ASDE, and AA of pre- and post-PI-treated cells were measured. Two Cytocapture dishes were used for each cell population, one loaded with nonPI-treated cells and the other with PI-treated cells.
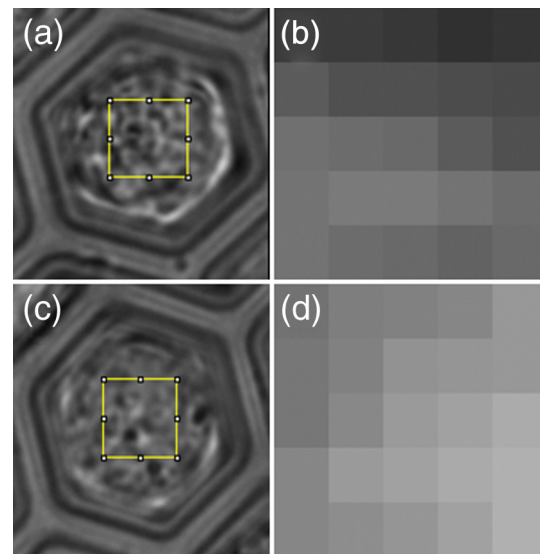
Fig. 3 Images (100$\times$, air immersion) and gray values. Images of dead (a) and live (c) cells, and their consequent gray value (b and d) displayed across a unit cell of 5×5 pixels, which is 1/400 of the respective region of interest (ROI) (100×100 pixels) defined by a square.
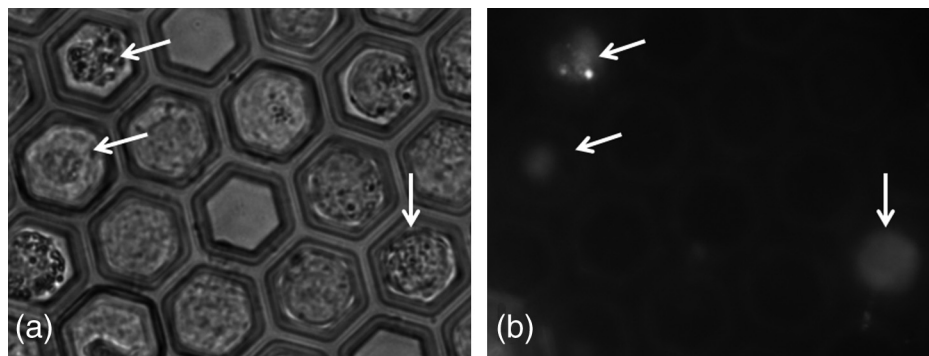
Fig. 2 U-937 cells within the Cytocapture dish (100$\times$). (a) Transmitted light image of a field of PWs. (b) Propidium iodide (PI) florescence image of the same field of PWs. Arrows indicate PI positive dead cells.
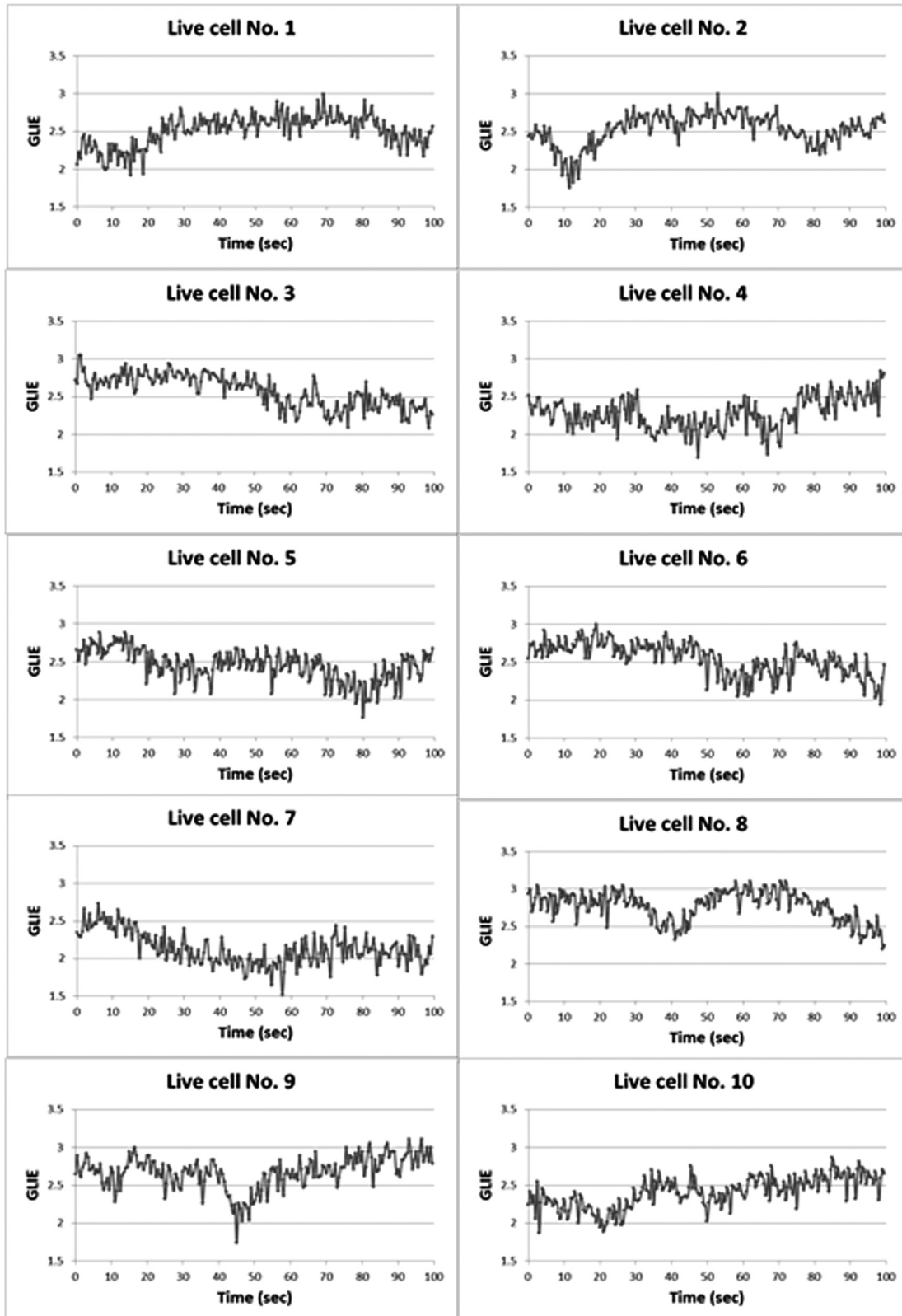
Fig. 4 Ten individual live-cell gray level information entropy (GLIE) time dependencies. Abscissa: time in seconds. Ordinate: GLIE values of cell unit (5 × 5 pixels).

Cell images and consequent gray values within a unit cell (i.e., 5 × 5 pixels) of representative dead and live cells are shown in Fig. 3. The ROI (100 × 100 pixels) from which AGLIE, ASDE, and AA were extracted is indicated by a yellow square.

Representative unit cell images (5 × 5 pixels) of the dead and live cell samples were acquired 200 times at 0.5 s intervals. The consequent time-dependent GLIE values of randomly chosen 10 live and 10 dead cells are depicted in Figs. 4 and 5. The
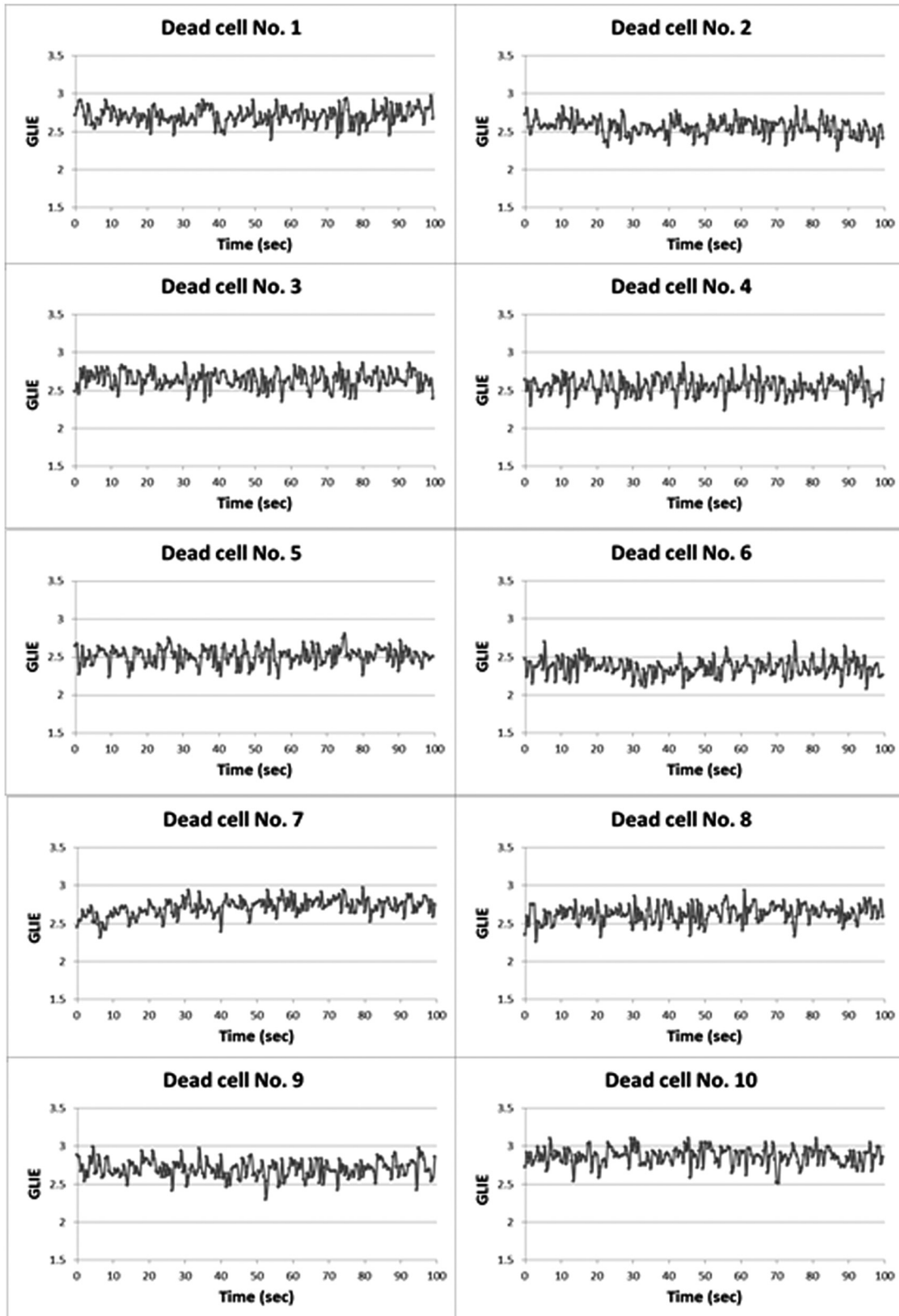
Fig. 5 Ten individual dead-cell GLIE time dependencies. Abscissa: time in seconds. Ordinate: GLIE values of cell unit (5×5 pixels).

corresponding 10-cells-based averaged power spectra (calculated with DFT) are presented in Fig. 6.

As seen in Figs. 4 and 5, and based on tens of additional corresponding measurements, the average GLIE value in live cells is lower than that in dead cells. Furthermore, there is no need for a closer look into the figures in order to notice the major difference between the two behaviors: The GLIE time dependencies of dead cells seem constant, while that of live
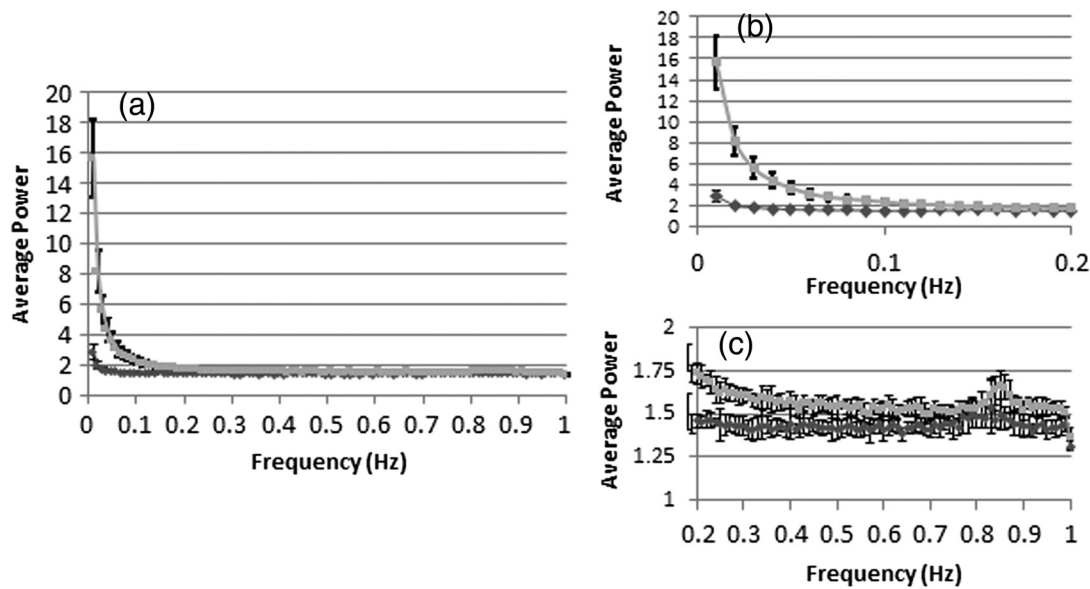
Fig. 6 Averaged power spectra of ten cells. For each frequency, the average power of 10 live and 10 dead cells were calculated and depicted in (a) (gray and black curves respectively). To better distinguish the deviation between the spectra, the data in (a) were divided into two frequency regions: (b) <0.2 Hz and (c) >0.2 Hz. Black bars depict standard deviation per frequency of 10 cells power spectra.

cells changes with time, indicating a possible periodic component. This is better recognized with the corresponding power spectra shown in Fig. 6. While the power spectra calculated from dead cell GLIE signals show no preference frequency (indicating complete randomness), that of live cells shows relatively notable powers at low frequencies. It is suggested that the fluctuate nature of higher frequency region powers reflects thermodynamic-based fluctuations of the cellular content, while the periodicity seen in GLIE signals in live cells (Fig. 6) reflects physiological metabolism. Obviously, the latter is expected to yield elevated SD and non-negligible autocorrelation values.

For the sake of clarity, utilizing the acquired data of the cells discussed in Fig. 3, a three-dimensional (3-D) layout of aGLIE25, SD25, and A25 is depicted in Fig. 7 at the single cell (5×5 pixel) resolution. Hence, each figure consists of 400 (20×20) data points, where their height (z coordinate) represents the value of the relevant measure, processed from 5×5 pixels of a unit cell, acquired 200 times at 0.5 s intervals. The location of a unit cell within an ROI (20×20 matrix of unit cells) is defined by their X, Y coordinates.

A close look at Fig. 7 reveals that while the difference between the aGLIE25 3-D presentations of dead and live cells (upper panel of Fig. 7) seems quite vague, it is clear in the SD25 and A25 3-D presentations.

After completion of the image acquisition procedure for the nonPI-stained sample, the same cells were stained with PI on a Cytocapture dish, and thereafter, underwent image acquisition a second time. By comparing results obtained for each of the measures before and after PI staining, all on the same cells, the performance of the measures in differentiating between dead and live U-937 cells could be determined at an individual cell resolution. Values of AGLIE, ASDE, AA, and consequent sensitivities and specificities, as concluded from the above comparison, are summarized in Table 1.

Frequency distributions of ASDE and AA values in live ($N = 192$) and dead ($N = 205$) cell populations (of Table 1) are presented in Fig. 8.

Clearly, the distribution of the two parameters, ASDE and AA for both dead and live cells, presents a negligible overlap, hence differentiating quite sharply between dead and live cells.

Examination of the results so far indicates the value of the proposed fluctuation-based measures ASDE and AA over that of the static measure AGLIE. Results in Table 1 indicate that the former yield better sensitivity or specificity in distinguishing between live and dead cells. Moreover, these parameters seem to be indifferent to PI staining, a fact which renders this approach more user friendly.

The high values obtained for AGLIE in dead cells in comparison to those in live cells are suggestive of the decrease of morphologic homogeneity in dead cells. This is in agreement with results obtained by Wiedemann et al.[14] and known morphological changes which occur in apoptosis, such as dense appearance of cytoplasm, tightly packed organelles, and chromatin condensation.[19] However, when fluctuation-sensitive measures (ASDE and AA) are considered, it is clear that dead cells behave as their intracellular content—more consistently than live cells.

AA values in live-still samples (see Appendix Tables 5 and 6) are considerably low and in harmony with the low values of AA of dead cells (Table 1).

The difference between SD and autocorrelation values obtained for dead cells and between the corresponding values obtained for live cells appears to be an unwavering phenomenon (this is so as it seems typical of most unit cells (5×5 pixels) within a ROI, when comparing between the two presentations of the middle panel and between the two presentations of the lower panel, both in Fig. 7). These high autocorrelation and SD values, as well as the cyclic behavior of GLIE (Figs. 4 and 5) are believed to stem from physiological activities occurring in live cells.

Dead cell   Live cell

(a)   (b) aGLIE

(c)   (d) SD25

(e)   (f) A25
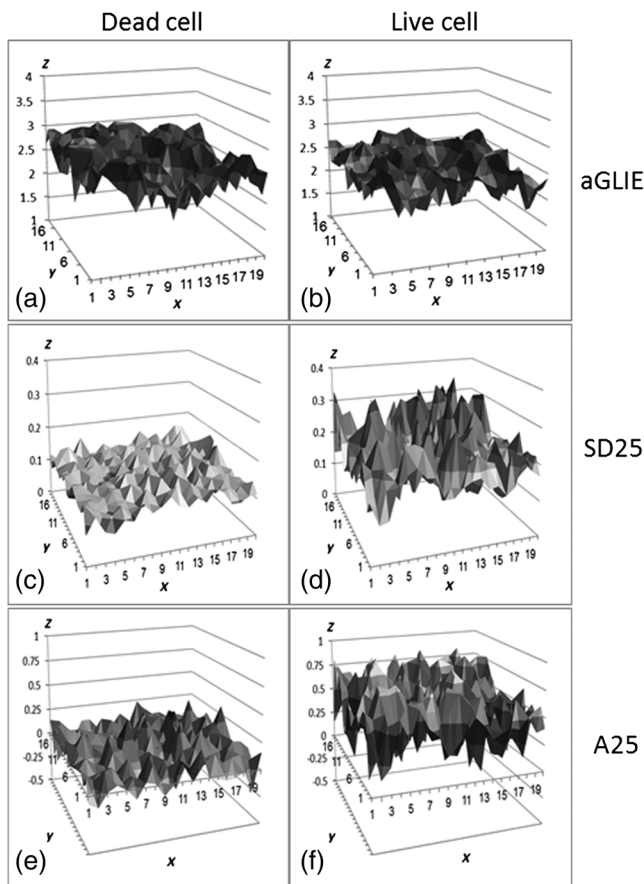
Fig. 7 Three-dimensional (3-D) layout of aGLIE25 (time-averaged GLIE25 over the 200 measurements of the same unit cell), SD25 and A25 in ROIs of representative dead [left column, (a), (c), and (e)] and live [right column (b), (d), and (f)] cells. Each figure consists of 400 data points (20×20). The Z coordinate stands for the value of the relevant measure processed from 5×5 pixels which assemble a unit cell. The location of a unit cell within the 20×20 unit cell matrix is defined by its X, Y coordinates. From top to bottom: aGLIE25, SD25, and A25.

Similar performances of ASDE and AA were observed in U-937 cells when measured at 60× magnification (see Appendix Table 7).

AGLIE, ASDE, and AA were also challenged with mixed (live and dead) cell populations of U-937 cells. The percentage

(a)   (b)
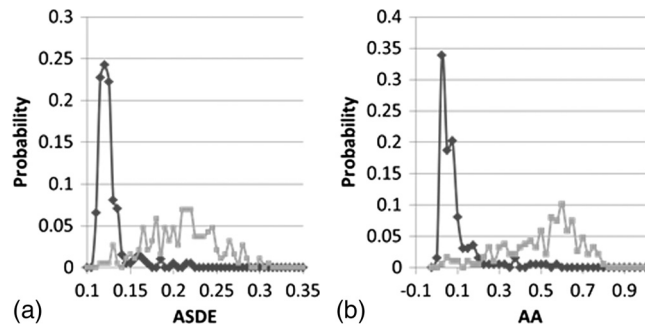
Fig. 8 Distribution of averaged temporal standard deviation (ASDE) (a) and average autocorrelation (AA) (b) values in dead (black curve) and live (gray curve) cell populations.

of dead and live cells in a given sample was practically predetermined by mixing certain volumes of 100% dead cell suspension with a certain volume of 97% live cell suspension at the same cell density. Three samples were prepared consisting of 100%, 50%, and 20% dead cells (cell solutions which contained 50% and 20% dead cells were prepared by mixing live and dead cells solutions at ratios of $1:0.94$, and $1:0.164$ v/v, respectively).

Results obtained by employing the measures were verified by counting the percent of PI positive cells are presented in Table 2:

As presented in Table 2, unlike with AGLIE, distinguishing between live and dead cells using ASDE and AA was found to be in high agreement with that of PI staining.

ASDE, AA, and DFT analyses of GLIE measured in resting nondifferentiated promonocytic U-937 cells before and after stimulation with PMA, and of dead U-937 cells, were calculated, and results presented in Table 3.

These results indicate statistically significant differences in all parameters between U-937 cells treated for 24 h with and without PMA. Results clearly imply that the AP of PMA-treated-cells is significantly higher than that measured in dead and live cells. Though quite likely, there is not enough evidence to suggest a direct relation between high AP and enhanced cell activity.

Distribution histograms of aGLIE25, SD25, and A25 values in 10 dead, 10 live normal, and 10 PMA-treated U-937 cells were examined as well, and their graphic presentations are

Table 1 Ability of averaged gray level information entropy (AGLIE), averaged temporal standard deviation (ASDE), and average autocorrelation (AA) to distinguish between dead and live U-937 cells, pre- and post-PI-treatment. *N*—number of cells.

Pre-PI	Live cells ($N = 120$)	Dead cells ($N = 99$)	*p* value	Sensitivity (%)	Specificity (%)
AGLIE	2.34 ± 0.11	2.53 ± 0.08	$<10^{-5}$	85	83
ASDE	0.21 ± 0.03	0.13 ± 0.01	$<10^{-5}$	95	95
AA	0.49 ± 0.15	0.09 ± 0.08	$<10^{-5}$	94	93

Post-PI	Live cells ($N = 72$)	Dead cells ($N = 106$)	*p* value	Sensitivity (%)	Specificity (%)
AGLIE	2.51 ± 0.08	2.64 ± 0.09	$<10^{-5}$	82	86
ASDE	0.21 ± 0.04	0.12 ± 0.01	$<10^{-5}$	95	93
AA	0.51 ± 0.19	0.04 ± 0.07	$<10^{-5}$	96	93

Table 2 Performance of AGLIE, ASDE, and AA in evaluating percentage of dead/live cells arrested within the Cytocapture dish. 100%, 50%, and 20% refer to estimated predetermined mixtures. *N*—number of cells in each group.

Parameter	100% ($N = 102$)	50% ($N = 114$)	20% ($N = 177$)
PI	1	0.526316	0.220339
AGLIE	0.813725	0.622807	0.248588
ASDE	0.970588	0.54386	0.225989
AA	0.970588	0.552632	0.220339

Table 3 Effect of PMA on U-937 cells evaluated by ASDE, AA, and discrete Fourier transform (DFT) of GLIE. *N*—number of cells in each group. AP—average power amplitude of frequency range <0.5 Hz.

Measure	Dead	Live ($N = 36$)	Live+PMA ($N = 29$)	*p* value dead-live	*p* value live-live + PMA-
ASDE	0.13 ± 0.03	0.27 ± 0.04	0.29 ± 0.02	$<10^{-5}$	0.004
AA	0.14 ± 0.17	0.70 ± 0.11	0.75 ± 0.04	$<10^{-5}$	0.04
AP	1.70 ± 0.43	3.12 ± 0.48	3.73 ± 0.45	$<10^{-5}$	$<10^{-5}$

displayed in Fig. 9, each panel showing 10 distribution curves of 10 individual cells. Calculation of said measures is performed from 100×100 pixels of an arbitrary selected ROI in the center region of each of the cells, yielding the histograms. A single curve is constructed from 400 relevant values, each extracted by processing the 5×5 pixels (data points) of a unit cell within a ROI.

As seen in Fig. 9, a high similarity is evident between curve shapes of individual cells within each cell group. Moreover, in addition to the significant differences between the mean values of the three groups (see also Tables 1 and 3), the respective shapes of distribution histograms are distinctive. Dead cell aGLIE25 curves (upper left panel) and A25 curves of both live cells incubated without (lower middle panel) and with PMA (lower-right panel) are skewed to the right. These skewed distributions may be asymmetric due to a natural limit (upper panel) of these parameters (maximum values of 3.22 and 1 for the aGLIE25 and A25, respectively) which prevent outcomes on one side. However, it is clear that the SD25 measure (middle panels, left to right) is significantly different not only in the mean value [0.12 ± 0.001 for the dead U-937 cell group, and respectively 0.21 ± 0.009 and 0.29 ± 0.02 for cells incubated without and with PMA ($p < 0.0001$), but in the dispersion of the values as well; for instance, the averaged SDs of SD25 values of cells incubated without and with PMA are 0.057 ± 0.006 and 0.063 ± 0.005 respectively, while that of dead cells are 0.02 ± 0.003; $p < 0.0001$ for both live cell groups versus dead cells]. Thus, the variability of SD25 within the 400 cell units of live cells is significantly higher than that within dead cells.

Moreover, histograms of SD25 derived from individual live cells treated with and without PMA exhibited low kurtosis

(1.18 ± 0.7 and 3.60 ± 1.03 respectively) in comparison with that of dead cells (24.42 ± 4.84; $p < 0.0001$). Similarly, skewness values for live cells treated with and without PMA (1.45 ± 0.18 and 2.21 ± 0.17 respectively) were found to be lower than those of dead cells (4.82 ± 0.44; $p < 0.0001$).

The differences among the above four parameters (ASDE, the standard deviation of the frequency distribution of SD25 within a ROI, and the skewness and kurtosis of these distributions) in live and dead cells are suggested to be attributed to the higher versatility of live cell content due to their physiology and inherent activity.

3.3 Generality of Averaged Temporal Standard Deviation of Entropy and Averaged Autocorrelation Measures

In order to assess the generality of the proposed fluctuation-based measures ASDE and AA, they were applied to other cell types as well: Jurkat, Molt-4 T-lymphoblast, and embryonic HEK293. Calculations were performed as with U-937cells above, and results are presented in Table 4.

The fact that the results in Table 4, obtained for Jurkat, Molt-4, and HEK293 cell lines, are consistent with those observed when applied to U-937 cell lines illustrates the generality of the proposed measures ASDE and AA.

3.4 Postulates and Foundations

The assumption on which this study relies is that intracellular physiological activities are associated with consequent spatiotemporal optospectroscopic alterations, which is, in turn, reflected in the appearance of time-dependent gray values within the transmitted light image of the examined cell. The main aim in this section is to present evidence to support said postulate in light of the results obtained.

The feasibility and system performance measurements performed on cell-free solutions (see Appendix) indeed strengthen this line of thought, as it teaches that these fluctuation-based measures, which are expected to report on the fluctuate nature of a measurement, are indifferent to static states such as various illumination intensities, deviations from proper object settings in respect to the microscope working plane, as well as the type of hosting media. On the other hand, the static parameter AGLIE, indeed, shows (Tables 5, 6, and Fig. 10) some level of sensitivity to these static states. It is, hence, suggested that this inherent difference between fluctuation-based and static measures makes the former more appropriate for distinguishing between still-life, dead and live cells, and between yes/no activated cells, disregarding the influence of static states, all clearly demonstrated in this study.

Results obtained on cells in the different states, dead, live, and PMA-activated, strengthen said postulate and furthermore, show positive correlation between the level of cell vitality and activity and the proposed fluctuation-based measures. In other words, the more active the cell, the greater the ASDE, AA, and AP values are.

Optical fluctuations in the cell image are related to fluctuations of cell content, refractive index, and permittivity, which are connected to fluctuation in mass density. With respect to the biological system, fluctuations in mass density can be attributed to both cell physiological activity and to inherent thermal Brownian fluctuations.

Dead cells **non-PMA cells** **PMA cells**
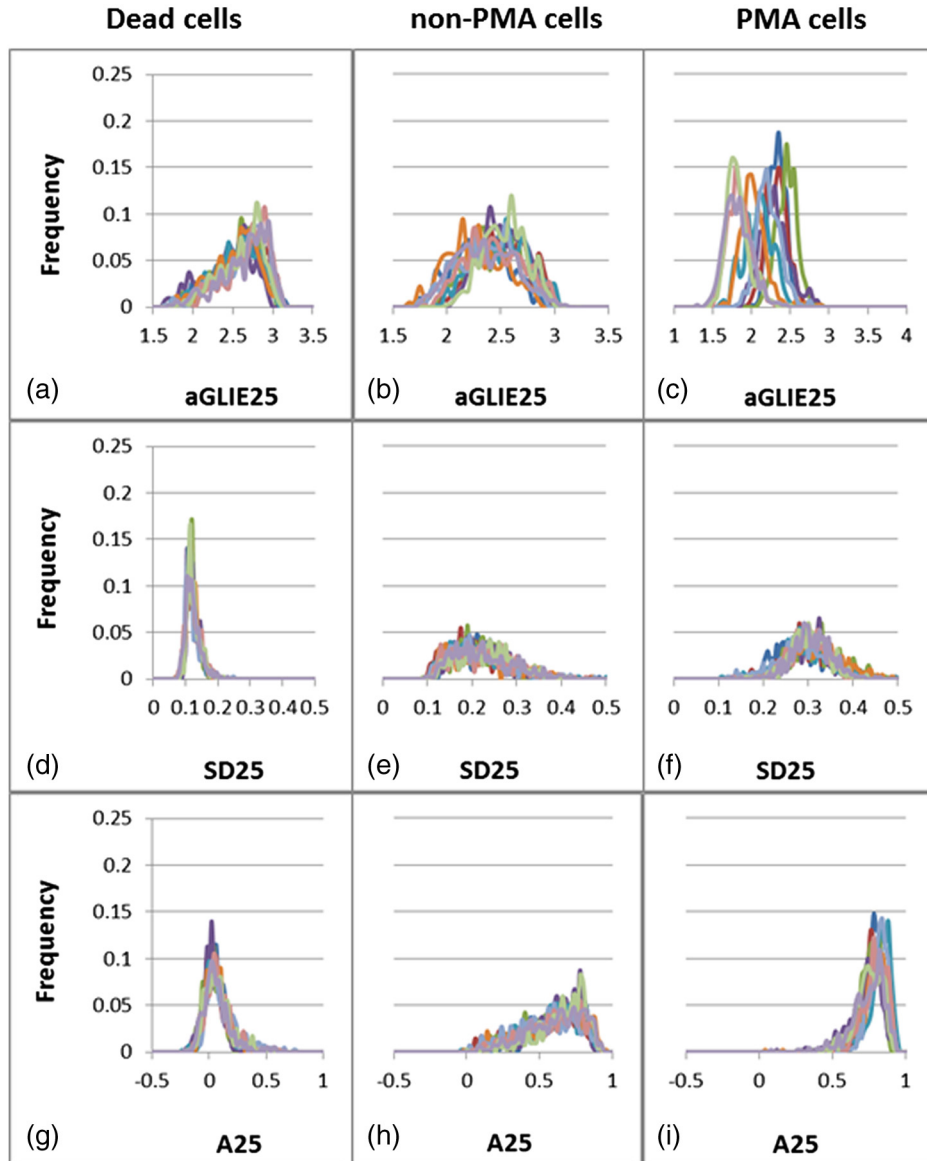
Fig. 9 Distribution histograms of (top to bottom) aGLIE25, SD25, and A25 measured in 10 representative individual cells: dead [(a), (d), and (g)], live incubated without PMA [(b), (e) and (h)] and with PMA p(c), (f) and (i)]. Each panel contains 10 occurrence curves, each of a different cell. Calculations of said measures are performed on 100×100 pixels of an arbitrary selected ROI, apparently within the center of the image of each of the cells, yielding the occurrence curves (histograms). A single curve is constructed from 400 relevant values, each extracted by processing the 5×5 pixels (data points) of a unit cell within a ROI.

Considering live cell in a physiological medium as a canonical thermodynamic system with temperature and volume reservoirs, statistical mechanics state that fluctuation ($\bar{\Delta}$) in mass density (ρ) can be expressed as: $\overline{(\Delta\rho)^2} = \rho^2 K_B T \beta_T / \Delta V$, where K_B is the Boltzmann constant, T is the temperature, and β_T is the isothermal compressibility.[20] This was further successfully applied on liquids[21,22] and suspensions of liposomes.[23,24]

On the other hand, since permittivity ε and refractive index n are mass-density and temperature-dependent, fluctuation in the latter two is expected to produce fluctuation in the permittivity and refractive index of a liquid medium as is generally expected, and in intracellular content as well, following the equation:[21,22]

$$\overline{(\Delta\varepsilon)^2} = \left(\frac{\partial n^2}{\partial \rho}\right)_T^2 \overline{(\Delta\rho)^2} + \left(\frac{\partial n^2}{\partial T}\right)_\rho^2 \overline{(\Delta T)^2}.$$

The dominant contributor to $\overline{(\Delta\varepsilon)^2}$ is density fluctuation $\overline{(\Delta\rho)^2}$ resulting from molecule motions, which contribute about 99% in comparison to just 1% contributed by temperature fluctuation.[22]

Fluctuation in cell permittivity was evident in measuring the time dependency of light scattered from cells.[25,26] Furthermore, it has been shown that these fluctuations in the refractive index range from 0.04 to 0.1 around $n = 1.35$ and that these fluctuations have long range spatial correlations.[26]

Table 4 Performance of ASDE and AA in distinguishing between live and dead cells within populations of Jurkat, Molt-4, and HEK293 cells.

Jurkat cell line	Live cells ($N = 65$)	Dead cells ($N = 15$)	*p* value	Sensitivity (%)	Specificity (%)
ASDE	0.23 ± 0.04	0.14 ± 0.01	$<10^{-5}$	100	95
AA	0.57 ± 0.12	0.17 ± 0.10	$<10^{-5}$	100	95

Molt-4 cell line	Live cells ($N = 52$)	Dead cells ($N = 29$)	*p* value	Sensitivity (%)	Specificity (%)
ASDE	0.23 ± 0.03	0.12 ± 0.02	$<10^{-5}$	97	100
AA	0.60 ± 0.12	0.04 ± 0.11	$<10^{-5}$	97	100

HEK293 cell line	Live cells ($N = 62$)	Dead cells ($N = 24$)	*p* value	Sensitivity (%)	Specificity (%)
ASDE	0.22 ± 0.03	0.13 ± 0.01	$<10^{-5}$	96	95
AA	0.61 ± 0.13	0.12 ± 0.11	$<10^{-5}$	92	95

Table 5 Influence of illumination-intensity upon AGLIE, ASDE, and AA [averaged over measurements of 10 picoliter wells (PWs)] with relevant *p* values below.

Measure	0	30%	80%	100%
AGLIE	1.52 ± 0.004	1.88 ± 0.012	2.24 ± 0.016	2.32 ± 0.016
ASDE	0.153 ± 0.001	0.154 ± 0.001	0.157 ± 0.016	0.159 ± 0.016
AA	0.009 ± 0.006	-0.0008 ± 0.005	0.026 ± 0.04	0.04 ± 0.04
	p	p	p	
	(0%–30%)	(30%–80%)	(80%–100%)	
AGLIE	$<10^{-5}$	$<10^{-5}$	$<10^{-5}$	
ASDE	0.002	0.307642	0.601502	
AA	0.0008	0.06	0.37	

Table 6 AGLIE, ASDE, and AA values measured in two types of liquids.

Measure	Water	Medium	*p* value
AGLIE	1.76 ± 0.05	1.83 ± 0.06	$<10^{-5}$
ASDE	0.159 ± 0.005	0.159 ± 0.001	0.88612
AA	0.08 ± 0.04	-0.005 ± 0.004	0.096175

At present, the time scale along which the proposed fluctuation-based measures are reliable and truly reflect cellular events relies on others' work. Joshi et al.[27] and Shaked et al.[28] have independently demonstrated, using different methods, fluctuations in phase values in living cells occurring in time scales of tens of milliseconds or more, which could be tracked and related to physiological changes. Joshi et al. initiated cellular physiological events by exposing cells to hypotonic media known to induce various cellular changes such as water influx into the cell, cell excitation, hormone release, migration, cell proliferation, and cell death.[29] Shaked et al., in applying their measurement system, followed *in vitro* physiological changes which occur during cardiomyocyte contraction-relaxation cycles.

Within the same time scale of tens of milliseconds or more, Watson et al.[30] showed random fluctuations of forward scattered light from living cells at the single cell level which yielded fluctuation in up to 30% of the scattered intensity.

In light of these studies, it can be assumed, with a high level of confidence, that the acquisition time used in the current work (~1 ms) does not average a representative fluctuation which lasts about tens of milliseconds or more, based independently on the work of Joshi et al., Shaked et al., and Watson et al. Now, since the time scale of several cardinal physiological processes, such as protein synthesis and translocation, is a few seconds,[31,32] it is anticipated that a sampling rate of 200 per 100 s (2 Hz) with sampling duration of 1 ms will be enough to trace these physiological events. This is also in agreement with Nyquist sampling criterion (Wolfarm MathWorld), which requires a sampling rate of at least twice the frequency of the function signal one wishes to reconstruct.

The GLIE measure seems to change quite periodically with cycle times longer than 10 s. (Figs. 4 and 5). It is suggested that this might be associated with the well-known physiological oscillations of the intracellular spatial concentration of signaling molecules,[33] and hence in turn, with the subsequent spatiotemporal fluctuation in mass density as well.

Following this line of thought, the time period of other intracellular oscillations may reach minutes and even hours.[34] However, some oscillations of pivotal intracellular mediators like Ca^{++}-induced translocation of protein kinase C and G proteins have been shown to take place in time periods of seconds.[35–37]

The above discussion is limited to pointing out various cellular constellations which could be monitored by the proposed fluctuation-based measures and does not purport to characterize any specific association between the biological event and said
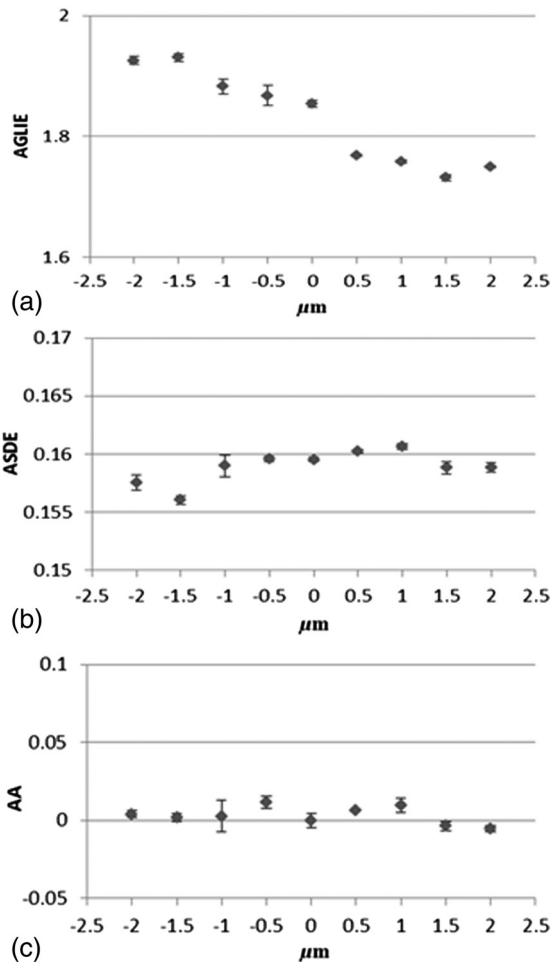
Fig. 10 Influence of deviation from proper sample-placement (in respect to the working plane distance) on (a) AGLIE, (b) ASDE, and (c) AA Each symbol in the figure represents the relevant three PW-based average value ± SD for a given distance (μm) of the object/sample from the microscope working plane ($z = 0$), wherefrom the object image is focused. Abscissa: distance (μm) from working plane ($z = 0$). Increment along the optical axis is 0.5 μm. Ordinate: (a), (b), and (c) are AGLIE, ASDE, and AA, correspondingly.

measure—a mission which calls for further investigation and analysis beyond the scope of the present study.

4 Summary

Spatiotemporal fluctuation of GLIE was investigated and realized in distinguishing among dead, live, and PMA-activated cells. This was performed on four types of cells by utilizing a combination of (a) simple bright-field microscope-based static cytometry and (b) Cytocapture dish, in which cells of interest are held, each within a picoliter optical chamber (20-μm entrance diameter, 8 μm depth), forming an arrayed cell arrangement which allows time-dependent measurement at individual-cell resolution while treated *in situ*.

Results obtained in this study indicate that fluctuation-sensitive measures (SD25/ASDE and A25/AA) seem to be more practical than static measures (GLIE25/AGLIE) in distinguishing between dead and live cells. Furthermore, relying on their good performance in distinguishing between cells activated with or without PMA, it is believed that the proposed ASDE and AA

measures might be a significant addition to the existing microscope-based probe-free toolbox.

It is our intention to further deepen this research by challenging the proposed measures to discriminate between various fine physiological states, under controlled induction and inhibition of intracellular processes.

Last but not least, the proposed ASDE and AA measures are eventually consequences of fluctuations of the index of refraction. The latter is a macroscopic parameter, and hence the ability of the measures to directly discover biophysical cause and its spatial aspect (which in some cases might be addressed by fluorescence microscopy) is justly questioned, even though indications of uneven spatial distribution of the proposed measures within a cell image have been observed, suggesting that they might reveal spatial information (data not shown). However, it is believed that an effort to correlate between the measures and between specific cellular situations, with established biochemical–physical aspects and location, might better define the ability of the measures to specifically identify cellular events, their location, and probably, to explore their biophysical mechanism as well. This effort might even be further enhanced if performed with higher contrast methods such as phase contrast microscopy, differential interference contrast, or quantitative phase imaging/digital holographic microscopy, which will probably have higher signal-to-noise ratio in comparison to the presently used bright field measurements.

Appendix

A.1 Dependency of averaged gray level information entropy, averaged temporal standard deviation, and average autocorrelation upon light intensity

A microscope Halogen lamp was used to evaluate the influence of light intensity upon the three measures. Intensities used were 0: no light (lamp is off), 30%, 80% (determined by means of natural density filters), and 100% of the source. Then AGLIE, ASDE, and AA were calculated for each of the intensities, in 10 PWs. The 10 PW-based averages are summarized in Table 5.

As seen in Table 5, the increase of AGLIE with light intensity is prominent ($p < 10^{-5}$), while ASDE and AA seem to be indifferent to measured intensity. This makes the latter two measures more appropriate for evaluating true changes occurring in cells, since they allow attribution of measured changes to intracellular physiological alteration or fluctuation, rather than to fluctuation in illumination intensity which can occur in microscopy on a regular basis.

The physical reasoning behind these findings, ignoring sources of electrical noise, is mostly photon statistics, according to which the expected SD equals the square root of the count $\sqrt{N}$. This means that the number of at least 68% of the gray values (1 SD) is $2\sqrt{N}$. For instance, if the average count read is 100, one would expect reading counts in the range of 90 to 110 with coefficient of variation (CV) of $\sqrt{N}/N = 10\%$, yielding 20 gray levels (within 1 SD). However, for average count read of say 10,000, $\sqrt{N} = 100$, yielding 200 gray values, though the entire relative distribution of gray values is narrowed (having CV of $\sqrt{N}/N = 1\%$). This was also verified by counting the number of gray values within ROIs at different intensities (data not shown). Hence, the higher

the intensity (N) (i.e., the higher $\sqrt{N}$), the wider the occurrence distribution of gray values, which results in higher values of GLIE. This explains the sensitivity of AGLIE to intensity, as shown in Table 5.

For clarification, when all 25 pixels (5×5 pixels) within a unit cell have the same gray value (maximum order), the occurrence of this single gray value within a unit is unity ($25/25$). Using Eq. (1), the GLIE25 of such a state is $-(25/25)\ln(25/25) = 0$. On the other hand, if each of the pixels has a different gray value (maximum disorder), the GLIE25 is $-25(1/25)\ln(1/25) = 3.22$. Therefore, in the particular case of a unit cell consisting of 25 pixels, $0 \leq \text{GLIE25} \leq 3.22$, this calculated range is in agreement with the measured right edge upper panel of the experimental frequency histogram curve of GLIE depicted in the upper panel of Fig. 9.

A.2 Influence of incorrect vertical sample-placement upon averaged gray level information entropy, averaged temporal standard deviation, and average autocorrelation

The influence of deviation from correct sample placement in respect to the microscope working and/or focal plane was examined. Experiments were performed on Cytocapture dishes loaded with medium, after assuring that the image of PW edges was focused. Then the Z coordinate of the microscope controlled stage was manipulated from $+2 \rightarrow -2$ in increments of 0.5 μm. All together, there were 9 Z-planes in each of which data was acquired (200 serial images) in 3 PWs. Results, AGLIE (1.83 ± 0.07), ASDE (0.159 ± 0.002), and AA (0.007 ± 0.015), indicate the indifference of the measures, especially those of ASDE and AA, to the vertical sample location within the said Z range. For a graphic illustration, see Fig. 10. A broader range of error was not considered due to its improbability of occurrence with an experienced user.

A.3 Dependency of averaged gray level information entropy, averaged temporal standard deviation, and average autocorrelation on liquid type

Utilizing the data acquisition and image processing procedures described above, AGLIE, ASDE, and AA was examined in 20 PWs, 10 per Cytocapture dish filled by either medium or water. Average values given in Table 6 indicate that liquid types are indistinguishable by both ASDE and AA, but might be distinguished by AGLIE. When attempting measurement of cells in suspension, the lower the interference of the hosting media with the applied measure, the more reliable and informative the measure is.

Table 7 ASDE and AA values in U-937 cells measured at 60× and 100× magnifications.

	U-937 cells 60× ($N = 36$)	U-937 cells 100× ($N = 24$)	*p* value 60× – 100×
ASDE	0.27 ± 0.04	0.27 ± 0.03	0.54
AA	0.70 ± 0.11	0.68 ± 0.09	0.34

A.4 Averaged temporal standard deviation and average autocorrelation parameter values at 60× and 100× magnifications

Live U-937 cells were measured for ASDE and AA values at 60× magnification and 100× magnification for comparison. Results are presented in Table 7.

No significant difference in ASDE and AA values was found between cells measured at 60× magnification and corresponding cells at 100× magnification.

References

1. B. N. G. Giepmans et al., "The fluorescent toolbox for assessing protein location and function," *Science* **312**, 217–224 (2006).
2. D. Evanko, "Label-free microscopy," *Nat. Methods* **7**(1), 36–36 (2010).
3. N. Pavillon, K. Fujita, and N. I. Smith, "Multimodal label-free microscopy," *J. Innovative Opt. Health Sci.* **7**(5), 1330009 (2014).
4. M.-N. Zhang, Y.-T. Long, and Z. Ding, "Filming a live cell by scanning electrochemical microscopy: label-free imaging of the dynamic morphology in real time," *Chem. Cent. J.* **6**(20), 1–6 (2012).
5. A. Rosenfeld and E. Troy, "Visual texture analysis," Technical Report 70-116, Computer Science Central, University Maryland, College Park, Maryland (1970).
6. A. Rosenfeld and M. Thurston, "Visual texture analysis, 2," Technical Report 70-129, Computer Science Central, University Maryland, College Park, Maryland (1970).
7. E. B. Troy, E. S. Deutsch, and A. Rosenfeld, "Gray-level manipulation experiments for texture analysis," *IEEE Trans. Syst. Man Cybernet.* **SMC-3**(1), 91–98 (1973).
8. R. M. Haralick, K. Shanmugam, and I. Dinstein, "Textural features for image classification," *IEEE Trans. Syst. Man Cybernet.* **SMC-3**(6), 610–621 (1973).
9. I. Pantic, S. Pantic, and J. Paunovic, "Aging increases nuclear chromatin entropy of erythroid precursor cells in mice spleen hematopoietic tissue," *Microsc. Microanal.* **18**(5), 1054–1059 (2012).
10. I. Pantic, S. Pantic, and G. Basta-Jovanovic, "Gray level co-occurrence matrix texture analysis of germinal center light zone lymphocyte nuclei: physiology viewpoint with focus on apoptosis," *Microsc. Microanal.* **18**(3), 470–475 (2012).
11. I. Pantic and S. Pantic, "Germinal center texture entropy as possible indicator of humoral immune response: immunophysiology viewpoint," *Mol. Imaging Biol.* **14**(5), 534–540 (2012).
12. I. Pantic et al., "Nuclear entropy, angular second moment, variance and texture correlation of thymus cortical and medullar lymphocytes: grey level co-occurrence matrix analysis," *An. Acad. Bras. Cienc.* **85**(3), 1063–1072 (2013).
13. R. C. Gonzalez and R. E. Woods, 3rd ed., *Digital Image Processing*, pp. 425–427, Prentice Hall, New Jersey (2008).
14. P. Wiedemann et al., "In situ microscopic cytometry enables noninvasive viability assessment of animal cells by measuring entropy states," *Biotechnol. Bioeng.* **108**(12), 2884–2893 (2011).
15. P. C. W. Davies, E. Rieper, and J. A. Tuszynski, "Self-organization and entropy reduction in a living cell," *BioSystems* **111**(1), 1–10 (2013).
16. D. Marín, M. Martín, and B. Sabater, "Entropy decrease associated to solute compartmentalization in the cell," *BioSystems* **98**(1), 31–36 (2009).
17. E. Schrödinger, *What is Life? The Physical Aspect of the Living Cell*, Cambridge University Press, Cambridge (1967).
18. B. Derrida, "Non-equilibrium steady states: fluctuations and large deviations of the density and of the current," *J. Stat. Mech.* **2007**(07), P07023 (2007).
19. A. Saraste and K. Pulkki, "Morphologic and biochemical hallmarks of apoptosis," *Cardiovasc. Res.* **45**(3), 528–53 (1999).

20. R. K. Pathria and P. D. Beale, "The grand canonical ensemble," Chapter 4 in *Statistical Mechanics*, p. 104, Elsevier, Butterworth-Heinemann, Oxford (2011).

21. A. Morel, "Optical properties of pure water and pure sea water," in *Optical Aspects of Oceanography*, N. G. Jerlov and E. S. Nielsen, Eds., pp. 1–24, Academic Press, New York (1974).

22. X. Zhang and L. Hu, "Estimating scattering of pure water from density fluctuation of the refractive index," *Opt. Express* **17**(3), 1671–1678 (2009).

23. R. Krivanek, L. Okoro, and R. Winter, "Effect of cholesterol and ergosterol on the compressibility and volume fluctuations of phospholipid-sterol bilayers in the critical point region: a molecular acoustic and calorimetric study," *Biophys. J.* **94**(9), 3538–3548 (2008).

24. P. Chong, M. Sulc, and R. Winter, "Compressibilities and volume fluctuations of archaeal tetraether liposomes," *Biophys. J.* **99**(10), 3319–3326 (2010).

25. S. L. Jacques, "Optical properties of biological tissues: a review," *Phys. Med. Biol.* **58**(11), R37–R61 (2013).

26. M. Xu, T. T. Wu, and J. Y. Qu, "Unified Mie and fractal scattering by cells and experimental study on application in optical characterization of cellular and subcellular structures," *J. Biomed. Opt.* **13**(2), 024015 (2008).

27. B. Joshi et al., "Label-free route to rapid, nanoscale characterization of cellular structure and dynamics through opaque media," *Sci. Rep.* **3**, 2822 (2013).

28. N. T. Shaked et al., "Whole-cell-analysis of live cardiomyocytes using wide-field interferometric phase microscopy," *Biomed. Opt. Express* **1**(2), 706–719 (2010).

29. F. Lang et al., "Functional significance of cell volume regulatory mechanisms," *Physiol. Rev.* **78**(1), 247–306 (1998).

30. R. Y. D. Watson et al., "Elastic light scattering from single cells: orientational dynamics in optical trap," *Biophys. J.* **87**(2), 1298–1306 (2004).

31. R. Young and H. Bremer, "Polypeptide-chain-elongation rate in Escherichia coli B/r as a function of growth rate," *Biochem. J.* **160**(2), 185–194 (1976).

32. J. F. Presley et al., "ER-to-Golgi transport visualized in living cells," *Nature* **389**(4), 81–85 (1997).

33. P. Paszek, D. A. Jackson, and M. R. H. White, "Oscillatory control of signalling molecules," *Curr. Opin. Genet. Dev.* **20**(6), 670–676 (2010).

34. A. Hoffmann et al., "The IkappaB-NF-kappaB signalling module: temporal control and selective gene activation," *Science* **298**(5596), 1241–1245 (2002).

35. E. Oancea and T. Meyer, "Protein kinase C as a molecular machine for decoding calcium and diacylglycerol signals," *Cell* **95**(3), 307–318 (1998).

36. F. Codazzi, M. N. Teruel, and T. Meyer, "Control of astrocyte Ca^{2+} oscillations and waves by oscillating translocation and activation of protein kinase C," *Curr. Biol.* **11**(14), 1089–1097 (2001).

37. L. Giri et al., "A G-protein subunit translocation embedded network motif underlies GPCR regulation of calcium osscillations," *Biophys. J.* **107**(1), 242–254 (2014).

Ishay Wohl is a PhD student of biophysics at Bar Ilan University's, Physics Department in Israel. He earned his medical degree at Tel Aviv University's, Sackler School of Medicine in 1992 and completed residency in plastic surgery at Jerusalem's Shaare Zedek Medical Center in 2000. Since then, he has been employed as a senior plastic surgeon at Klalit Health Services, and a senior physician at the Plastic Surgery Units of Kaplan Medical Center in Rehovot and Barzilai Medical Center in Ashkelon.

Mordechai Deutsch is a member of the Physics Department at Bar Ilan University. He formulated the vision of the Biophysical Interdisciplinary Jerome Schottenstein Center for the research and technology of the cellome, established it and serves as its director. His fields of expertise are molecular physics, biophysics, electromagnetism, geometric and physical optics, fluorescence, micro optics, light microscopy, advanced imaging and signal analysis, microfluidics, and micro fabrication. Applications include spectroscopic measurements of live cells in cancer, immunology, and cryobiology.

Biographies for the other authors are not available.